BRAIN
A JOURNAL OF NEUROLOGY

Impaired plasticity of macrophages in X-linked adrenoleukodystrophy

Isabelle Weinhofer,[1] Bettina Zierfuss,[1] Simon Hametner,[2,3] Magdalena Wagner,[1,4] Niko Popitsch,[5,6] Christian Machacek,[7] Barbara Bartolini,[8] Gerhard Zlabinger,[9] Anna Ohradanova-Repic,[7] Hannes Stockinger,[7] Wolfgang Köhler,[10] Romana Höftberger,[11] Günther Regelsberger,[11] Sonja Forss-Petter,[1] Hans Lassmann[2] and Johannes Berger[1]

X-linked adrenoleukodystrophy is caused by ATP-binding cassette transporter D1 (*ABCD1*) mutations and manifests by default as slowly progressive spinal cord axonopathy with associated demyelination (adrenomyeloneuropathy). In 60% of male cases, however, X-linked adrenoleukodystrophy converts to devastating cerebral inflammation and demyelination (cerebral adrenoleukodystrophy) with infiltrating blood-derived monocytes and macrophages and cytotoxic T cells that can only be stopped by allogeneic haematopoietic stem cell transplantation or gene therapy at an early stage of the disease. Recently, we identified monocytes/macrophages but not T cells to be severely affected metabolically by ABCD1 deficiency. Here we found by whole transcriptome analysis that, although monocytes of patients with X-linked adrenoleukodystrophy have normal capacity for macrophage differentiation and phagocytosis, they are pro-inflammatory skewed also in patients with adrenomyeloneuropathy in the absence of cerebral inflammation. Following lipopolysaccharide activation, the ingestion of myelin debris, normally triggering anti-inflammatory polarization, did not fully reverse the pro-inflammatory status of X-linked adrenoleukodystrophy macrophages. Immunohistochemistry on post-mortem cerebral adrenoleukodystrophy lesions reflected the activation pattern by prominent presence of enlarged lipid-laden macrophages strongly positive for the pro-inflammatory marker co-stimulatory molecule CD86. Comparative analyses of lesions with matching macrophage density in cases of cerebral adrenoleukodystrophy and acute multiple sclerosis showed a similar extent of pro-inflammatory activation but a striking reduction of anti-inflammatory mannose receptor (CD206) and haemoglobin-haptoglobin receptor (CD163) expression on cerebral adrenoleukodystrophy macrophages. Accordingly, ABCD1-deficiency leads to an impaired plasticity of macrophages that is reflected in incomplete establishment of anti-inflammatory responses, thus possibly contributing to the devastating rapidly progressive demyelination in cerebral adrenoleukodystrophy that only in rare cases arrests spontaneously. These findings emphasize monocytes/macrophages as crucial therapeutic targets for preventing or stopping myelin destruction in patients with X-linked adrenoleukodystrophy.

1 Department of Pathobiology of the Nervous System, Center for Brain Research, Medical University of Vienna, Vienna, Austria
2 Department of Neuroimmunology, Center for Brain Research, Medical University of Vienna, Vienna, Austria
3 Institute of Neuropathology, University Medical Center Goettingen, Germany
4 Department of Clinical Science, Intervention and Technology; Karolinska Institutet, Stockholm, Sweden
5 Wellcome Trust Centre for Human Genetics, University of Oxford, UK
6 Children's Cancer Research Institute, Vienna, Austria
7 Institute for Hygiene and Applied Immunology, Center for Pathophysiology, Infectiology and Immunology, Medical University of Vienna, Vienna, Austria
8 Department of Laboratory Medicine, Medical University of Vienna, Vienna, Austria
9 Institute of Immunology, Medical University of Vienna, Vienna, Austria
10 Department of Neurology, University Hospital Leipzig, Leipzig, Germany
11 Institute of Neurology, Medical University of Vienna, Vienna, Austria

Correspondence to: Johannes Berger
Center for Brain Research, Medical University of Vienna
Spitalgasse 4, A-1090 Vienna, Austria
E-mail: johannes.berger@meduniwien.ac.at

Introduction

With an estimated overall frequency of 1:17 000, X-linked adrenoleukodystrophy (X-ALD, OMIM #300100) is a rare inherited disorder that is characterized by the destruction of myelin sheaths that normally protect and insulate nerve fibres in the CNS (Moser *et al.*, 2001). X-ALD shows a striking phenotypic heterogeneity. The severe inflammatory form (cerebral ALD, CALD), often of childhood onset, exhibits rapidly progressive, fatal cerebral demyelination with disruption of the blood–brain barrier and infiltration of immune cells, mainly monocytes/macrophages and CD8+ T cells. The milder default manifestation of X-ALD is adrenomyeloneuropathy (AMN), characterized by slowly progressive non-inflammatory adult-onset spinal cord axonopathy with associated demyelination. All X-ALD phenotypes are caused by mutations in the *ABCD1* gene encoding the peroxisomal ATP-binding cassette transporter subfamily D, member 1 (ABCD1, formerly ALDP). Thus, a dysfunctional ABCD1 protein is necessary but not sufficient to initiate the disastrous cerebral inflammation in patients with X-ALD. The biochemical function of ABCD1 is the import of coenzyme A-activated saturated very long-chain fatty acids (VLCFAs) into peroxisomes, where they are degraded by β-oxidation (van Roermund *et al.*, 2008, 2011; Wiesinger *et al.*, 2013). Accordingly, the pathognomonic abnormality of X-ALD is the accumulation of VLCFAs in body fluids and tissues of patients (Moser *et al.*, 2001). How the excess of VLCFAs contributes to X-ALD pathogenesis and what kind of environmental or possibly genetic or epigenetic factors trigger the start of the rapidly progressive demyelination in CALD remains largely unclear (Berger *et al.*, 2014; Wiesinger *et al.*, 2015).

Currently, the only treatment option to halt the devastating course of CALD is allogeneic haematopoietic stem cell transplantation or gene therapy using *ex vivo* genetically corrected CD34 + stem cells, when performed at an early stage of the disease (Cartier and Aubourg, 2010). To understand why haematopoietic stem cell transplantation or gene therapy stops the inflammation in CALD, we recently determined the extent of the metabolic defects of the different CD34 + -derived immune cell populations from patients with X-ALD and identified monocytes, in which *ABCD1* is normally highly expressed, as metabolically most severely affected by X-ALD in terms of β-oxidation and VLCFA accumulation (Weber *et al.*, 2014). Monocytes

are circulating blood phagocytic cells that are part of the peripheral innate immune system. Upon CNS injury, monocytes respond to chemotactic factors by passing the blood–brain barrier and migrating to sites of tissue damage. There, monocytes differentiate into macrophages and, together with CNS-resident microglial cells, initiate defence mechanisms aiming to clear the injured site by producing neurotoxic cytokines and reactive oxygen species and by phagocytosing myelin debris. The uptake of myelin directly affects the function of macrophages by inducing an anti-inflammatory polarization state, which promotes tissue regeneration and remyelination (Boven *et al.*, 2006; Prinz and Priller, 2014). Thus, under neurodegenerative conditions, macrophages and microglia are thought to exert dichotomous functions by participating in both tissue destruction and repair.

Myelin-laden macrophages are prominent in active CALD lesions (Powers *et al.*, 1992). Nevertheless, the inflammatory reaction in CALD is not self-limiting but proceeds progressively resulting in almost complete loss of brain myelin. Thus, the situation in CALD is in stark contrast to other disorders characterized by inflammatory demyelination, such as multiple sclerosis, which typically displays a relapsing-remitting course. This prompted us to hypothesize that ABCD1 deficiency alters the function of monocytes and macrophages towards an intrinsically skewed, pro-inflammatory state, rendering them unable to acquire the anti-inflammatory polarization state necessary to dampen the destruction of myelin and to initiate repair. In line with this assumption, a recent study demonstrated alterations in the lipid-driven pro-inflammatory cascades of glycosphingolipid and glycerophospholipid synthesis in peripheral blood mononuclear cells isolated from patients with AMN (Ruiz *et al.*, 2015). In post-mortem CALD brains, a zone lacking microglia was found in perilesional white matter immediately beyond the actively demyelinating lesion edge (Eichler *et al.*, 2008). Like monocytes and macrophages, microglial cells are important phagocytes necessary for removal of myelin debris and for initiating recruitment of oligodendrocyte precursor cells. Accordingly, a decimation of microglia would even further necessitate proper monocyte/macrophage function in the context of CALD. Thus, the aim of the present study was to characterize the plasticity of monocytes and macrophages in X-ALD by comprehensive analyses of circulating blood monocytes and differentiated macrophages *in vivo* and

in vitro, before and after myelin phagocytosis, to understand their particular role in the pathology of X-ALD.

Materials and methods

Patients and healthy volunteers

The study included peripheral blood samples from seven patients with AMN (age 23–45 years, mean = 35 years) and 19 healthy volunteers (age 25–61 years, mean = 38 years), all males of Caucasian origin. All recruited AMN patients displayed clinical symptoms of axonopathy in the spinal cord but no signs of cerebral involvement at brain MRI. White blood cell counts, obtained at the time of sampling, did not reveal any signs of inflammation. None of the patients received medication, including Lorenzo's oil, for treatment of neurological symptoms. However, in five patients, adrenocortical insufficiency was managed by steroid replacement therapy. The accumulation of VLCFAs in the blood of patients with AMN was confirmed by measurement of the total amount of the fatty acids C26:0, C24:0, C22:0 and, for normalization, C16:0 by using gas chromatography–mass spectrometry (GC–MS) as described (Weber *et al.*, 2014). The study was approved by the Ethical Committee of the Medical University of Vienna (EK1462/2014) and informed consent was obtained from participating AMN patients and healthy volunteers. Immunohistochemistry was performed on postmortem CNS tissue from five X-ALD (*n* = 3 childhood CALD, *n* = 1 adult CALD, *n* = 1 AMN) and six acute multiple sclerosis cases. Patient characteristics and conditions are listed in Supplementary Table 1. Use of this material was approved by EK729/2010 and EK535/2016.

Isolation and lipopolysaccharide stimulation of human monocytes

Blood was collected by venipuncture under fasting conditions into heparin tubes and CD14 + monocytes were isolated by magnetic-activated cell sorting (MACS) using CD14 microbeads (Miltenyi Biotec) as described (Weber *et al.*, 2014). The purity of the cells was measured by flow cytometry using FITC-coupled mouse antibodies directed against human CD3 and CD14 (Miltenyi Biotec; Supplementary Fig. 1). For lipopolysaccharide (LPS) stimulation, monocytes were plated onto uncoated 12-well culture plates (3×10^6 cells/well) in RPMI complete medium [RPMI 1640 supplemented with 2 mM L-glutamine, 100 μg/ml streptomycin, 100 U/ml penicillin (all Invitrogen) and 10% heat-inactivated LPS-free foetal calf serum (FCS) (Gibco Life Technologies)] and stimulated for 6 h with either 0.5 ng/ml or 10 ng/ml LPS (Sigma).

RNA isolation and reverse transcription-coupled quantitative PCR analysis

RNA isolation and reverse transcription-quantitative PCR (RT-qPCR) analysis was carried out as previously described (Weber *et al.*, 2014). Cells were lysed in TRIzol® following the manufacturer's (Invitrogen) instructions and homogenized by passing through a QIAshredder spin column (Qiagen). The isolated total RNA fraction was purified using RNeasy® Mini Kit and RNase-free DNase digestion (Qiagen). RNA concentration was measured using a Nanodrop spectrophotometer (Peqlab), and total RNA (100 ng) was reverse transcribed using the iScript™ cDNA Synthesis Kit (Bio-Rad). The cDNA was amplified in technical duplicates by RT-qPCR using the SsoFast™ Eva Green® Supermix (Bio-Rad) and the primers listed in the Supplementary Table 2. Relative transcript abundance was detected by SYBR Green incorporation and calculated by the $2^{-\Delta\Delta Ct}$ method using GAPDH as internal reference for normalization. HPRT and HMG20B were detected using the TaqMan™ method and SsoFast™ Probes Supermix (Bio-Rad). Each sample was measured in two technical replicates.

Transcription profile of monocytes from patients with adrenomyelo-neuropathy and healthy controls

For whole-transcriptome analysis of mRNA expression, RNA was extracted from freshly isolated CD14 + monocytes of five patients with AMN and five healthy control subjects as described above, and 3 μg total RNA was used for the generation of mRNA-focused libraries. The samples were sequenced on a HiSeq2000 sequencing system (Illumina) at the Biomedical Sequencing facility of the Medical University of Vienna, Austria. This resulted in 16–36 million 50 nucleotide (nt) long reads per sample. Reads were mapped to the UCSC GRCh37 (hg19) reference genome with TopHat v 2.0.12 (K *et al.*, 2013) using the UCSC Ensembl gene annotations. TopHat was configured with standard parameters except for setting the seed length to 15 and the maximum number of multi-hits to 100; expected inner distance between mate pairs was set to 190. Read mapping resulted in an average of 28 million aligned reads (97.74–98.25%) per sample. Count-tables were created with HTSeq v0.6.0 (Anders *et al.*, 2015). Differential expression between different sample groups was calculated using edgeR v3.6.8 and DESeq v1.16.0, *P*-values were adjusted using Benjamini and Hochberg's algorithm to control the false discovery rate. Genes with adjusted *P*-values < 0.05 were considered as significantly deregulated unless stated otherwise. Heatmaps were created using the R 'heatmap' package, normalized read counts were calculated by dividing raw counts by DESeq-calculated size factors. Pathway analyses were conducted with the standard GSEA method (Subramanian *et al.*, 2005) as accessible at http://software.broadinstitute.org/gsea by entering lists of significantly deregulated genes. Results were then confirmed by using the more sophisticated 'GSEAPreranked' method. For this, a ranked list of all genes was created by setting the rank of a gene to sgn(logFC) × (1 / q) + logFC where logFC is the calculated log-fold change and q is the adjusted *P*-value as calculated by edgeR. GSEAPreranked tested this list for significant enrichment at the beginning and end of this list and the overlap with the standard GSEA results was checked manually.

Library-normalized read counts and the output from the used differential-expression tools EdgeR and DEseq are listed in Supplementary Tables 5 and 6.

Quantification of the phagocytic ability of monocytes

The phagocytic ability of monocytes was determined in whole blood samples using the pHrodo® Red *E. coli* BioParticles® Phagocytosis Kit (Life Technologies) according to the manufacturer's instructions. In brief, 100 μl of heparinized whole blood samples were incubated with 20 μl non-opsonized, fluorogenic *Escherichia coli* particles at 37°C or on ice (negative control) for 15 min. To stop phagocytosis, all tubes were placed on ice. Monocytes were distinguished from other phagocytosing immune cell types by forward- and side-scatter characteristics and by labelling with Pacific Blue™-conjugated CD14 monoclonal antibody for 30 min at room temperature in the dark. Fluorescence-activated cell sorting (FACS) analysis was carried on a FACScalibur™ Flow Cytometer (BD Bioscience) at the Core Facility of the Medical University of Vienna, Austria.

Viability and glutathione measurement of monocytes

The viability of monocytes was measured by the MultiTox-Glo Multiplex Cytotoxicity Assay and the glutathione red-ox balance was determined by the GSH/GSSG Glo Assay according to the manufacturer's instructions (both Promega). The detection was carried out using the Glomax detection system (Promega). For each assay 5×10^4 freshly isolated monocytes plated into opaque, white 96-well plates were used.

Determination of oxygen consumption in monocytes

Bioenergetic analyses were performed by XF24 Extracellular Flux Analyzer (Seahorse Biosciences) following the manufacturer's instructions. Monocytes were seeded at a density of 2.5×10^5 cells/well in an XF24 cell culture plate. Cells were allowed to adhere for 2 h in RPMI complete medium; 1 h before the bioenergetic assays were performed, culture medium was replaced by glucose-containing medium (Seahorse Biosciences). Cells were allowed to equilibrate at 37°C and then the basal oxygen consumption rate and the response to sequential incubation with oligomycin (0.5 μM), carbonyl cyanide-p-trifluoromethoxyphenylhydrazone (FCCP, 0.6 μM) and antimycin A (10 μM) was assessed.

In vitro differentiation of human CD14+ monocytes to macrophages

CD14+ monocytes were differentiated by seeding the cells at a density of 7.7×10^5 cells per well into 12-well plates in RPMI complete medium supplemented with either 50 ng/ml granulocyte-macrophage colony-stimulating factor (GM-CSF) or M-CSF (PeproTech) for 7 days to obtain M1-like pro-inflammatory or M2-like anti-inflammatory macrophages, respectively. The differentiated macrophages were further activated with 100 ng/ml LPS (Sigma) plus 25 ng/ml IFN-γ (PeproTech) or 100 ng/ml IL-4 (Novartis) for 2 days in the presence of either 10 ng/ml GM-CSF or M-CSF. The accumulation of VLCFAs in blood monocytes and *in vitro* differentiated macrophages was analysed by using GC–MS as described (Weber *et al.*, 2014).

Flow cytometry

In vitro differentiated macrophages were detached using 1.5 mM EDTA in Hanks' Balanced Salt solution (Invitrogen) and then washed with phosphate-buffered saline (PBS) containing 1% BSA and 0.02% NaN$_3$. Cells were blocked with 2.4 mg/ml human IgG (Beriglobin P) on ice for 30 min to prevent non-specific binding before the addition of monoclonal antibodies. The following monoclonal antibodies were used: Alexa Fluor® 700-conjugated anti-MHC class II monoclonal antibody (clone MEM-136, EXBIO); FITC-conjugated CD80 monoclonal antibody (clone 2D10); APC.Cy7-conjugated CD206 monoclonal antibody (clone 15-2); PerCP.Cy5.5-conjugated CD163 monoclonal antibody (clone GHI/61), PerCP.Cy5.5- and FITC-conjugated isotype control monoclonal antibody (clone MOPC21, all BioLegend). Samples were analysed on a LSRII flow cytometer (BD Biosciences) and the data were further processed with the FlowJo software (Treestar). Living single cells were gated according to their forward- and side-scatter characteristics and exclusion of dead cells using 4′,6-diamidino-2-phenylindole (DAPI) (Sigma).

Cytokine and free haemoglobin measurement

Cytokines were measured from cell-free supernatants via Luminex® technology using specific matched-pair antibodies and recombinant cytokines as standards (eBioscience). Free haemoglobin was measured in plasma samples using 3-wavelength spectrophotometry according to the method of Harboe (1959).

Myelin isolation

Myelin was isolated from whole brains of a total of 17 male 6–8-week-old wild-type (C57BL/6J) mice by ultracentrifugation according to the protocols of Norton and Poduslo (1973) and Larocca and Norton (2007). The isolated myelin was recovered in PBS, tested for putative LPS contamination using an Endotoxin detection kit (Lonza) and stored in aliquots at −80°C until use.

Western blot analysis

About 5 μg of isolated myelin and, as a control, 19 μg whole brain homogenate in 5× sample buffer [60 mM tris(hydroxymethyl)aminomethane (Tris)-HCl pH 6.8; 25% (w/v) glycerol; 2% (w/v) SDS; 5% (v/v) β-mercaptoethanol; 0.025% bromophenol blue] were loaded onto a 12% polyacrylamide gel for discontinuous sodium dodecyl sulphate polyacrylamide gel electrophoresis (SDS-PAGE) followed by blot transfer onto a nitrocellulose membrane. The membrane was probed at 4°C overnight with the following primary antibodies: rabbit polyclonal anti-ionized calcium-binding adapter molecule 1 (Iba-1; Thermo Scientific, 1:4000), rabbit monoclonal anti-synaptophysin (Epitomics, 1:4000) and rabbit polyclonal anti-proteolipid protein 1 (PLP1; Serotec, 1:10 000). The secondary goat anti-rabbit IgG antibody conjugated with horseradish peroxidase (Bio-Rad; 1:20 000) was detected by application of Immobilon Western HRP Substrate Peroxide Solution and Immobilon Western HRP Luminol Reagent (both Millipore)

using the ChemiDoc Imaging system and Image Lab software (Bio-Rad).

Fluorescent labelling of myelin and measurement of macrophage uptake by fluorescence-activated cell sorting

Isolated myelin was fluorescently labelled by incubating 1 mg myelin in PBS with 10 μl pHrodo®-Red succinimidyl ester dissolved in DMSO (1 mg/ml, Life Technologies) for 45 min at room temperature in the dark. Excess dye was removed by a short centrifugation and the labelled myelin was resuspended in PBS (pH 7.4) and stored in aliquots at −80°C. Differentiated macrophages were stimulated with 100 ng/ml LPS for 24 h and further incubated with 20 μg/ml pHrodo®-Red stained myelin for 6 or 24 h before FACS analysis.

Immunohistochemical analysis of post-mortem CNS tissue

Target, type, pretreatment, dilution and source of the primary antibodies used for immunohistochemistry are listed in Supplementary Table 3. Immunohistochemical single labelling targeting CD68, CD86, CD163, CD206 and MRP14 were performed as described (Hametner *et al.*, 2013) using the avidin-biotin complex method. Single labelling for CD86 additionally included a biotinylated tyramine amplification step (termed 'catalysed signal amplification' in Supplementary Table 3), which is described elsewhere (King *et al.*, 1997). For immunohistochemical double-labelling targeting CD86 + CD206, after pretreatment (see Supplementary Table 3) and blocking of unspecific background staining using 10% FCS diluted in Dako® wash buffer (Code number S3006) (FCS/DAKO), the primary antibodies were diluted in FCS/DAKO and applied simultaneously overnight at 4°C. The following day, sections for CD86 + CD206 staining were rinsed five times with Tris buffer (0.01 M, pH 8.5) and incubated with simultaneously applied secondary antibodies diluted in FCS/DAKO (biotinylated anti-goat antibody diluted 1:500; peroxidase-conjugated anti-mouse antibody diluted 1:100; both Jackson ImmunoResearch) for 60 min at room temperature. After a Tris buffer washing step, sections were incubated with avidin-alkaline phosphatase (Sigma, product code A-7294) diluted 1:500 in FCS/DAKO for 60 min at room temperature. Alkaline phosphatase labelling for CD86 was developed with Fast blue (blue precipitate) substrate (Sigma). Then, peroxidase labelling of CD206 was developed with 3-amino-9-ethyl-carbazole (Sigma, product code A5754). Sections were coverslipped with GelTol.

Statistical analysis

For comparison of matched pairs of AMN and healthy control derived monocytes that were isolated and treated in parallel on the same days, the Wilcoxon-signed rank test or the paired two-tailed Student's *t*-test were used. For statistical analyses of untreated monocytes, *in vitro* differentiated macrophages and immunohistochemical staining, the unpaired two-tailed Student's *t*-test was used. The *P*-value was calculated and the null hypothesis was denied when the *P*-value exceeded 0.05. All boxplots and dot plots were drawn using the R software

[www.r-project.org (Tippmann, 2015)], whereas bar graphs were generated with Microsoft Excel. The sample sizes were determined based on our preliminary data and all samples obtained were included in the analysis.

Results

Dysregulation of immunoregulatory pathways in adrenomyeloneuropathy monocytes predisposes for pro-inflammatory activation

First, we asked how ABCD1 deficiency affects the transcriptome of X-ALD monocytes. Thus, we purified CD14 + monocytes from peripheral blood of five AMN patients without brain inflammation (pure AMN; three patients received steroid replacement treatment for adrenocortical insufficiency), and five healthy controls. After establishing purity of the cells by flow cytometry (Supplementary Fig. 1), RNA was isolated for next-generation sequencing. Bioinformatic pathway analysis revealed the most significantly altered mRNA levels for genes related to inflammation such as cytokine-cytokine receptor interaction, chemokine signalling or NOD-like receptor signalling (Table 1, top). The expression pattern of two AMN patients (Patients P1 and P2) showed a pronounced upregulation of a specific set of genes that consisted of pro-inflammatory markers like *TNFA* or *IL1B* (Supplementary Fig. 2). This activation pattern was never observed in healthy control monocytes, analysed in parallel, and could also not be attributed to elevated erythrocyte haemolysis during handling (Supplementary Table 4), steroid replacement therapy, or any overt clinical changes in disease progression. To explore whether monocytes of some AMN patients are chronically particularly pro-inflammatory, we reinvestigated the highly activated Patient P2 around 2 years later. This reanalysis revealed activation similar to that of monocytes derived from the other AMN patients (Supplementary Fig. 3). Thus, we reasoned that a predisposition for temporary, pronounced activation of monocytes seem to be associated with X-ALD and could possibly vary with disease course-related factors like microscopic dysmyelinative foci in AMN brain tissue or subclinical urinary tract infection due to bladder dysfunction (Powers *et al.*, 2000; Hofereiter *et al.*, 2015).

We next hypothesized that the induction of pro-inflammatory genes in AMN monocytes could reflect a higher susceptibility for pro-inflammatory priming of these cells. To explore this possibility, we isolated monocytes pairwise from AMN patients and healthy controls, stimulated these with different concentrations of LPS *in vitro* and then analysed the induction of selected pro-inflammatory genes by RT-qPCR. When comparing the fold induction obtained by high (10 ng/ml) relative to low (0.5 ng/ml) dose LPS treatment, the AMN monocytes displayed significantly stronger increases in *TNFA*, *IL1B* and *IL6* mRNAs than healthy control cells treated in parallel (Fig. 1). These results

Table 1 Top five differentially regulated canonical pathways in AMN monocytes

KEGG pathway analysis	q-value
AMN patients *n* = 5, controls *n* = 5	
Cytokine-cytokine receptor interaction	2.64×10^{-11}
Chemokine signalling pathway	2.64×10^{-11}
NOD-like receptor signalling pathway	2.64×10^{-11}
Toll-like receptor signalling pathway	5.45×10^{-8}
Cytosolic DNA sensing pathway	1.37×10^{-5}
AMN patients *n* = 3, controls *n* = 5	
Chemokine signalling pathway	8.58×10^{-4}
Cytokine-cytokine receptor interaction	1.64×10^{-3}
MAPK signalling pathway	1.05×10^{-2}
Glycerophospholipid metabolism	2.33×10^{-2}
Insulin signalling pathway	2.75×10^{-2}

Top: Top 5 KEGG pathways that are significantly enriched with genes found to be differentially expressed between AMN patients and healthy controls (*n* = 5 each). Adjusted *P*-values ('q-value') were calculated with Gene Set enrichment analysis. *Bottom*: Top 5 KEGG pathways that are significantly enriched with genes found to be differentially expressed between AMN patients (excluding the 'activated' patient samples from Patients P1 and P2; *n* = 3) and healthy controls (Subjects C1–C5; *n* = 5). Adjusted *P*-values (q-value) were calculated with Gene Set enrichment analysis.

indicate that ABCD1 deficiency predisposes monocytes for pro-inflammatory activation.

The pronounced activation state of the original samples of AMN Patients P1 and P2 could potentially mask alterations in other important pathways associated with monocyte functions. However, a separate comparison of monocytes from AMN Patients P3–P5 and controls again revealed chemokine signalling and cytokine-cytokine receptor interaction as the most affected processes (Table 1, bottom). Hence, alterations in these pathways apparently occur in AMN monocytes, independent of acute inflammatory activation. Next, we filtered gene hits by differential expression and significance level between the AMN and healthy control groups and found 36 genes being significantly deregulated (Fig. 2A, Supplementary Tables 5 and 6). To verify the next-generation sequencing results, we applied RT-qPCR for selected mRNAs in an enlarged validation cohort; the results confirmed the statistically significant deregulation of five candidate genes (upregulated: ATP-binding cassette subfamily A member 1, *ABCA1*; C-C motif chemokine ligand 4, *CCL4*; suppressor of cytokine signalling 3, *SOCS3*; and purinergic receptor P2Y13, *P2RY13*; downregulated: krueppel like factor 10, *KLF10*) in AMN monocytes compared with healthy controls (Supplementary Fig. 4A). Furthermore, the mRNA level of the chemotactic gene C-X-C motif chemokine receptor 4 (*CXCR4*), which was close to the threshold for statistical significance in the RNA-Seq experiment, was significantly upregulated in AMN monocytes of the validation cohort (Supplementary Fig. 4B).

To reflect and corroborate the dysregulation of chemokine signalling found in AMN monocytes, we next investigated whether monocytes and macrophages accumulate in long ascending and descending spinal cord tracts of a well-characterized AMN case with primary axonal loss and associated demyelination (Budka *et al.*, 1976).

Immunohistochemistry for migration inhibitory factor-related protein 14 (MRP14), an early activation marker for monocytes/macrophages recently recruited to the CNS (Brück *et al.*, 1995) and CD68, a microglia/macrophage phagocytosis marker, revealed accumulation of MRP14 + and CD68 + monocytes/macrophages in perivascular cuffs around blood vessels of affected AMN spinal cord tracts (Fig. 2B), thus confirming previous investigations (Powers *et al.*, 2000). These results imply that in the AMN spinal cord, monocytes and macrophages are recruited to perivascular cuffs in affected tracts and accumulate there, thus reflecting the chemotactic pathway alterations of monocytes found in the RNA-Seq analysis (Fig. 2 and Table 1).

To evaluate other functional aspects of AMN monocytes, we also analysed their phagocytic ability, intracellular redox status, viability and mitochondrial oxidative phosphorylation (Supplementary Fig. 5). We observed no significant alterations in these parameters and, thus, conclude that although AMN monocytes possess a pro-inflammatory predisposition, other monocyte functions are not compromised.

Repolarization from a pro-inflammatory to an anti-inflammatory state is incomplete in adrenomyeloneuropathy macrophages

We next assessed how ABCD1 deficiency affects the differentiation of monocytes towards macrophages and to which extent the VLCFA accumulation in these cells is altered during the differentiation process. Accordingly, we differentiated monocytes from AMN patients and healthy controls *in vitro* to either pro- or anti-inflammatory macrophages by using either GM-CSF or M-CSF, respectively, followed by further activation with LPS plus IFN-γ (M1) or IL-4 (M2). FACS analysis revealed no statistically significant difference in the expression of pro- (MHC-II, CD80 and CD86) and anti-inflammatory (CD163 and CD206) cell surface markers between AMN and control samples (Fig. 3A). These results indicate that ABCD1 deficiency does not impair the ability for differentiation into either M1 or M2 polarized macrophages *per se*. However, when comparing cytokine levels in the supernatant of GM-CSF differentiated and LPS plus IFN-γ activated macrophages, we noticed a trend for increased production of the pro-inflammatory cytokines TNF-α, IL-1β, IL-12p40 and IL-23 in the M1-activated macrophages from AMN patients versus healthy controls (Fig. 3B). We then measured the total amount of the VLCFAs C26:0 and C22:0 and, for normalization, the long-chain fatty acid C16:0 in both monocytes and activated macrophages by GC–MS. As expected, the relative amount of C26:0, displayed as a ratio to either C22:0 or C16:0, was ∼7-fold higher in AMN blood monocytes compared with those of healthy controls (Fig. 3C). When comparing the levels of C26:0/C22:0 and C26:0/C16:0 of *in vitro* differentiated and activated macrophages, we found a 10–14-fold and 10–12-fold increase, respectively, in AMN cells over controls (Fig. 3C).
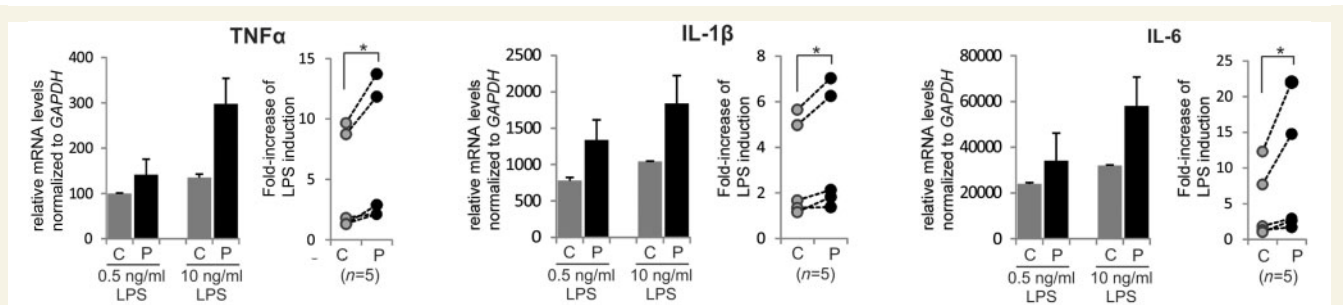
Figure 1 **Transcriptome analysis reveals dysregulation of inflammatory pathways in monocytes of AMN patients.** The complete transcriptome of primary CD14+ monocytes from AMN patients and healthy controls was obtained by RNA-Seq. RT-qPCR analysis of pro-inflammatory cytokine (*TNFA*, *IL1B* and *IL6*) expression in AMN and control monocytes cultured for 6 h with either 0.5 or 10 ng/ml LPS. See also Table 1. *Left*: Representative results of monocytes derived from one AMN patient and a matched healthy control, isolated and treated in parallel. Each bar represents the mean of two independent LPS treatments each measured in two technical replicates. *Right*: Pairwise comparisons (indicated by lines) of the response to LPS of AMN and corresponding healthy control monocytes isolated and treated in parallel (n = 5 each). The induction is depicted as the fold-increase in relative mRNA levels of *TNFA*, *IL1B* and *IL6* obtained by high LPS (10 ng/ml) relative to low LPS (0.5 ng/ml) concentration. The mRNA levels were normalized to *GAPDH*, which is not induced by LPS. *$P \leqslant 0.05$ (Wilcoxon-signed rank test); error bars = standard deviation; P = AMN patient; C = healthy control.

Accordingly, the high degree of VLCFA accumulation under conditions of ABCD1 deficiency is even further elevated upon differentiation of monocytes to macrophages; thus, also reflecting the induction of fatty acid synthesis as a driving force for phagocytic differentiation (Ecker *et al.*, 2010).

Phagocytosis of myelin is a robust anti-inflammatory stimulus inducing the alternative activation (M2) response in macrophages (Boven *et al.*, 2006; Prinz and Priller, 2014). Hence, we tested if AMN macrophages have an altered capacity for switching towards the anti-inflammatory M2 phenotype upon myelin phagocytosis. First, we ensured that the uptake of myelin, isolated from murine brain (Supplementary Fig. 6), was similar in AMN and healthy control macrophages (Fig. 4A). Then we activated *in vitro* differentiated macrophages with LPS and determined the mRNA levels of the pro-inflammatory genes *TNFA* and *IL12B* (IL-12p40) by RT-qPCR in response to myelin treatment. Without added myelin, the expression of both genes was markedly higher in AMN macrophages compared with healthy controls (Fig. 4B). Upon myelin ingestion, the fold decrease of *TNFA* and *IL12B*/IL-12p40 expression was comparable in AMN and healthy control macrophages (Supplementary Fig. 7), indicating that the pro-inflammatory status decreased also in X-ALD cells. However, the final level of expression in the AMN macrophages appeared much higher, with pro-inflammatory mRNA levels still approaching those seen in activated control macrophages without myelin treatment (Fig. 4C).

Comparison of the activation status of macrophages in active CNS lesions of cerebral adrenoleukodystrophy and multiple sclerosis

To confirm reduced plasticity of X-ALD macrophages *in vivo*, we used immunohistochemistry to compare the activation status of macrophages in cerebral demyelinating lesions of post-mortem brains from four CALD and six multiple sclerosis cases (Supplementary Table 1). Like CALD, multiple sclerosis is an inflammatory disease with primary demyelination in the CNS and prominent monocyte/macrophage as well as T cell infiltration (Powers *et al.*, 1992; Frischer *et al.*, 2009). However, in contrast to the relentless progression in CALD, multiple sclerosis typically displays a relapsing-remitting course.

In the profoundly inflammatory lesions of CALD brains, neutral lipid-containing late macrophages indicative of prior myelin phagocytosis are prominent. Accordingly, we selected acute multiple sclerosis cases with active inflammatory lesions comprising comparable densities of macrophages in general as well as similar amounts of neutral lipid-containing macrophages. At this stage of multiple sclerosis, anti-inflammatory markers are expressed in macrophages/microglia (Vogel *et al.*, 2013). Thus, for quantification of microglia/macrophage markers in both CALD and multiple sclerosis lesions, we selected regions with (i) high densities of microglia/macrophages in the CD68 staining; and (ii) high expression of the anti-inflammatory macrophage marker mannose receptor (CD206). We first counted infiltrating monocytes, macrophages and activated microglia in CALD and multiple sclerosis lesions. Accompanying rather late and comparable stages of myelin degradation in the CALD and multiple sclerosis lesions (presence of periodic acid-Schiff-positive myelin degradation products in macrophages), we observed significantly higher numbers of recently recruited MRP14+ cells (Fig. 5A) in CALD lesions than in multiple sclerosis lesions. This result might reflect a sustained ability of X-ALD monocytes to migrate to sites of injury, as also observed for AMN (Fig. 2B). Neither the density of cells positive for the pan macrophage/microglia marker CD68 nor for the pro-inflammatory marker CD86 was significantly different between CALD and multiple sclerosis lesions (Fig. 5A and B). Most importantly, the
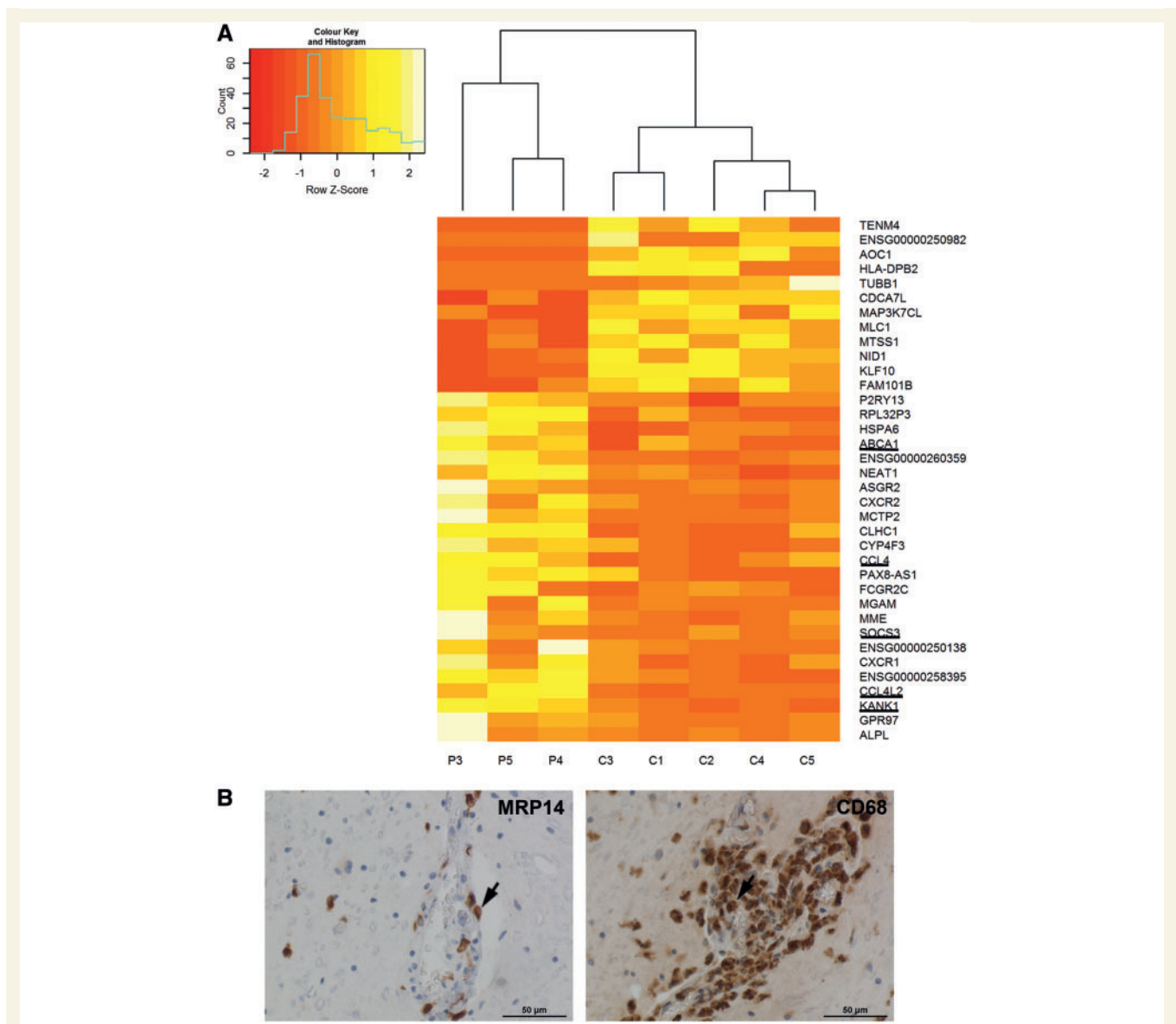
Figure 2 Deregulated gene expression pathways in AMN monocytes are reflected by recruitment of monocytes to perivascular cuffs in AMN spinal cord areas affected by myelopathy. (**A**) Heatmap of normalized read counts for genes found to be significantly deregulated in these cells. This list includes all genes with an adjusted *P*-value < 0.1 as determined by either edgeR or DESeq. Genes that were also deregulated in activated monocytes from AMN Patients P1 and P2 are underlined. P = AMN patient; C = healthy control. (**B**) Light microscopy images taken from the centre of cervical demyelinating lesions in post-mortem AMN spinal cord tissue. *Left*: Immunohistochemistry for MRP14 (early marker for activated monocytes/macrophages) detects infiltrating monocytes/macrophages. *Right*: Staining for the phagocytosis marker CD68 reveals the presence of macrophages and microglial cells. See also Table 1.

numbers of macrophages expressing the anti-inflammatory markers CD206 and haemoglobin-haptoglobin receptor (CD163) were significantly reduced in CALD lesions compared with multiple sclerosis lesions (Fig. 5A–C). For CD206, this also held true after normalization to the total (CD68 +) number of macrophages (Fig. 5A–C). Although lipid-laden macrophages, indicative of myelin phagocytosis, were abundant in CALD lesions, these macrophages were remarkably large—even for lipophages—and predominantly expressed pro-inflammatory CD86 but only low levels of anti-inflammatory CD206 (Fig. 5D). This was in stark

contrast to the activation of macrophages in multiple sclerosis lesions, where about half of CD86-positive cells also expressed CD206, thus showing an intermediate activation status (Fig. 5D).

Discussion

In X-ALD, monocytes/macrophages are metabolically the most severely affected immune cells (Weber *et al.*, 2014) and the dominant leucocytes in inflammatory demyelinating
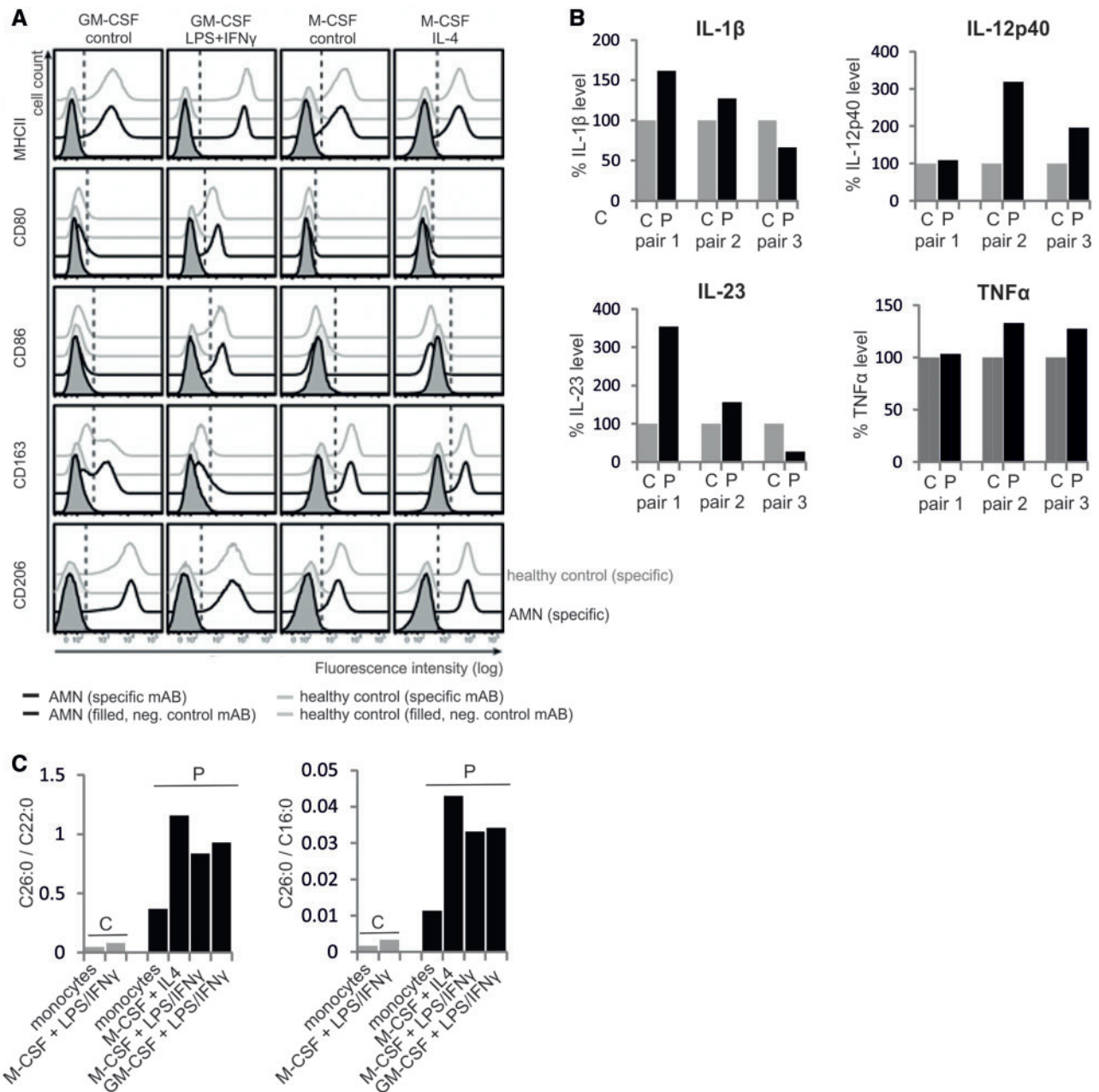
Figure 3 ABCD1 deficiency does not impair *in vitro* differentiation and pro- or anti-inflammatory polarization of monocyte-derived macrophages. (**A**) CD14+ monocytes isolated from the blood of AMN patients or healthy controls were differentiated with either GM-CSF or M-CSF for 7 days and subsequently either activated with LPS plus IFN-γ or IL-4, resulting in pro- or anti-inflammatory activation, respectively, or left untreated for additional 2 days. Pro-inflammatory (MHCII, CD80 and CD86) and anti-inflammatory (CD163, CD206) cell surface marker expression was assessed by flow cytometry. The dashed, vertical line represents the 1% threshold of the isotype control staining of AMN-derived macrophages. Histograms represent one out of three experiments with independent AMN and healthy control donor pairs. (**B**) Secreted levels of pro-inflammatory cytokines (TNFα, IL-1β, IL12p40 and IL-23) were measured in cell culture supernatants of LPS/IFN-γ activated GM-CSF differentiated macrophages, derived from blood monocytes isolated from three pairs of AMN patients and matched healthy controls and treated in parallel. The results are depicted with the level in patient samples relative to the matched controls (= 100%). (**C**) The concentrations of C26:0, C22:0 and C16:0 were determined by GC–MS in monocytes and *in vitro* differentiated and activated macrophages from one AMN patient and a matched healthy control. The relative amounts of C26:0 displayed as ratio to either C22:0 or C16:0 are shown. P = AMN patient; C = healthy control.
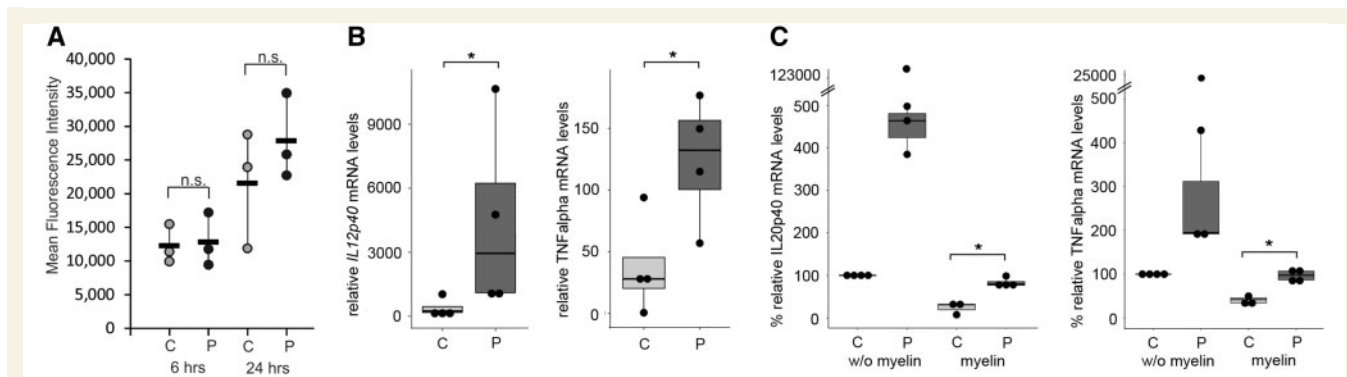
Figure 4 Macrophages derived from AMN patients only partially downregulate LPS-induced pro-inflammatory genes upon myelin phagocytosis. CD14 + bloodstream monocytes isolated from AMN patients or healthy controls were differentiated *in vitro* with M-CSF and subsequently activated with LPS for 24 h before incubation with or without myelin for additional 24 h. (**A**) The efficiency of myelin phagocytosis in AMN and healthy control macrophages was determined by FACS analysis after incubation with pHrodo®-Red labelled myelin for 6 h or 24 h. The mean fluorescence intensity of macrophages derived from isolated blood monocytes of three AMN patients and three healthy controls is depicted. *$P \leqslant 0.05$, n.s. = not significant (two-tailed unpaired Student's *t*-test). (**B** and **C**) The relative expression of *IL12B*/IL-12p40 and *TNFA* induced by LPS activation was measured by RT-qPCR without (**B**) or with (**C**) added myelin. The mRNA levels were normalized to the geometric mean of two reference genes, *HPRT* and *HMG20B*, which are not induced by LPS. In **C**, the normalized mRNA levels of control macrophages without myelin addition was set as 100%. For statistical analyses, logarithmic transformation was used to normalize the IL12B/IL-12p40 dataset. *$P \leqslant 0.05$ (two-tailed unpaired Student's *t*-test). P = AMN patient; C = healthy control.

brain lesions (Powers *et al.*, 1992). Here, we attempted to shed light on a detrimental role of these cells in the pathophysiology of X-ALD.

By applying whole transcriptome sequence analysis, we identified a pro-inflammatory skewing of the expression pattern in AMN monocytes, independent of the initiation of CALD symptoms. This intrinsic pre-activation profile, together with the increased propensity for full pro-inflammatory activation in response to LPS that we observed *in vitro*, is reflected *in vivo* by enhanced recruitment of monocytes/macrophages to perivascular cuffs at sites of myelopathy in AMN spinal cord. Importantly, in addition to the intrinsic activation profile due to ABCD1 deficiency, appropriate signalling from an active primary site of CNS injury, possibly by activated microglial cells, is required to attract recruitment of monocytes. Recently, Musolino and collaborators (2015) showed *in vitro* that the lack of ABCD1 in endothelial cells resulted in increased adhesion of co-cultured monocytic THP-1 cells and proposed a blood–brain barrier dysfunction in endothelial cells of X-ALD patients. Accordingly, our data complement this observation by showing that, in X-ALD, not only endothelial cells are dysfunctional but also monocytes appear to have an increased propensity to migrate to sites of CNS injury and, possibly, through the blood–brain barrier.

In contrast to the chemotactic pathway alterations observed in AMN monocytes, we were unable to detect significant deviations in other monocyte functions including phagocytic ability, viability, mitochondrial oxidative phosphorylation or intracellular redox status. The latter aspect contrasts with a recent observation by Turk and colleagues, who found a reduction of the total antioxidant capacity in monocyte lysates of both AMN and CALD patients (Turk *et al.*, 2017). However, in this report, the monocytes

were cultured for 7 days before analysis, possibly indicating that an imbalance in the oxidative status of X-ALD monocytes develop upon prolonged culture or is conceivable also upon differentiation to macrophages.

Concerning CALD, a critical question is why the transition of the inflammatory reaction in the brain, from an initially destructive pro-inflammatory phase to a proliferative remodelling phase aimed to halt demyelination and induce repair, is less efficient than in other demyelinating disorders like multiple sclerosis. We targeted this therapeutically important aspect by investigating the ability of X-ALD macrophages to polarize towards a deactivated, anti-inflammatory M2 phenotype upon phagocytosis of myelin. Indeed, our *in vitro* studies revealed that the pro-inflammatory skewing of X-ALD monocytes persists upon differentiation to macrophages. Furthermore, after the ingestion of myelin debris, the pro-inflammatory gene expression remained at a higher level than in control macrophages. Importantly, the immunohistochemical postmortem examination of CALD brain lesions reflected these findings. When compared to classically active lesions of acute multiple sclerosis cases, where macrophages display an intermediate activation status expressing both pro-inflammatory and anti-inflammatory markers (Vogel *et al.*, 2013), significantly fewer infiltrating macrophages expressed the anti-inflammatory markers CD206 and CD163 in CALD lesions (Fig. 5). Thus, although lipid-laden macrophages are generally observed in CALD lesions, these cells apparently have a reduced ability to adopt the anti-inflammatory polarization state that would induce repair processes. This drastically reduced number of anti-inflammatory macrophages/microglia might contribute to the lack of spontaneous halt of inflammation in most of the X-ALD lesions. In this context, however, it should be
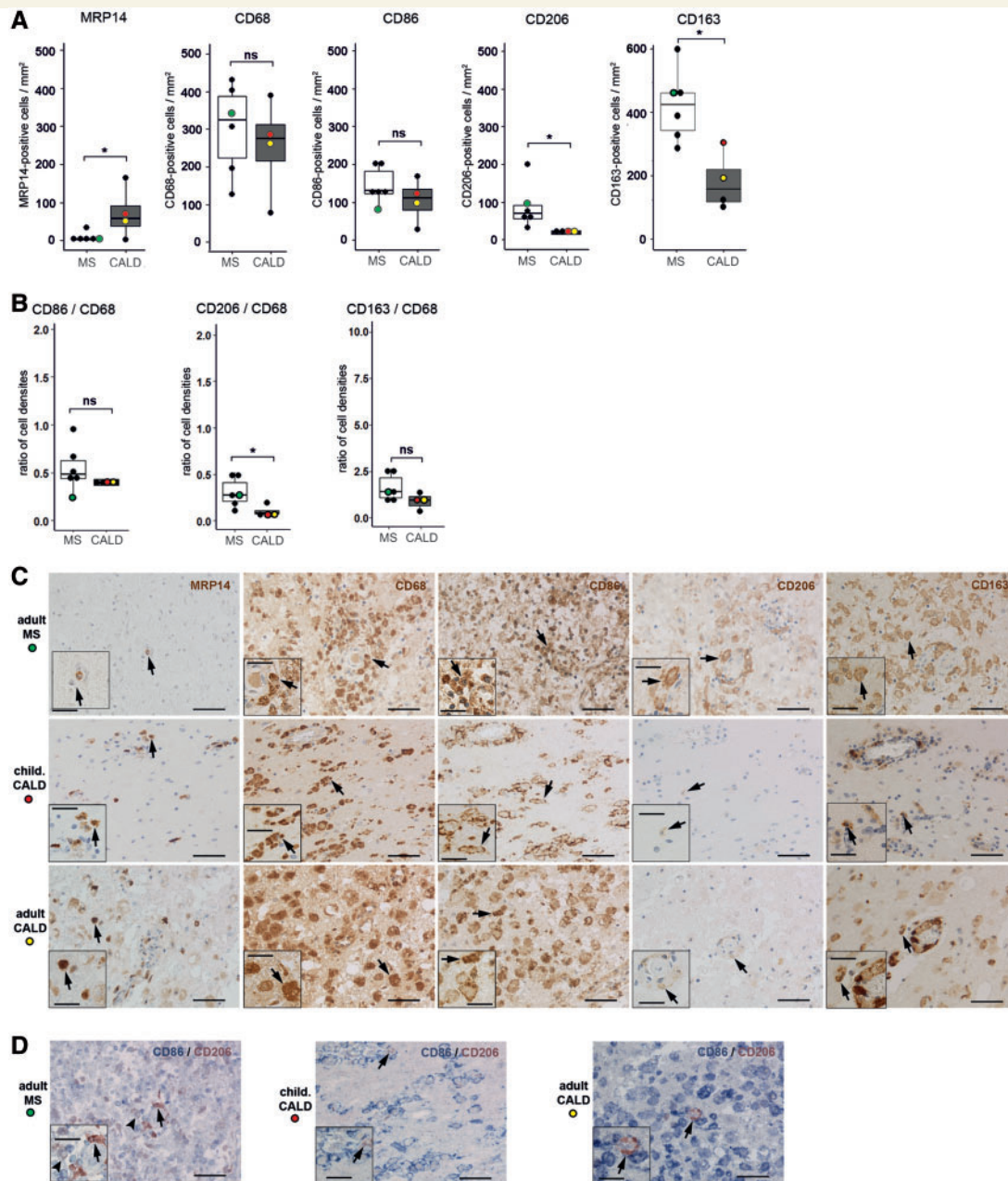
Figure 5 **Comparison of pro- and anti-inflammatory polarization markers on monocytes/macrophages and microglia in primary demyelinating CNS lesions in CALD and multiple sclerosis.** (**A**) Primary CALD (Cases 1 and 3, one tissue section per patient; Case 2, two tissue sections; Case 4, three tissue sections; $n = 4$ cases) and multiple sclerosis brain lesions (one tissue section per patient, $n = 6$ cases) were stained with antibodies directed against the early activation marker MRP14, the macrophage/microglia phagocytosis marker CD68, the pro-inflammatory surface marker CD86 and the anti-inflammatory surface markers CD206 and CD163. The number of positively stained cells in the centre of primary lesions was counted manually under the light microscope. The cell density is depicted as boxplot (median $\pm$ interquartile range) comparisons between multiple sclerosis and CALD. For cases where more than one tissue section was counted, the mean was used for calculation. For statistical analysis, logarithmic transformation was used to normalize the distribution of MRP14 and CD206 positive data sets. *$P \leqslant 0.05$ (two-tailed unpaired Student's t-test). Coloured dots indicate the cases used for immunohistochemistry in **C**: red dot = childhood CALD Case 2; yellow dot = adult CALD Case 4; green dot = multiple sclerosis Case 9. (**B**) Number of cells expressing the activation markers CD86, CD206 and CD163, respectively, in relation to the total number of CD68 positive macrophages in the counted fields. For statistical analysis, logarithmic transformation was used to normalize the ratio data. *$P \leqslant 0.05$ (two-tailed unpaired Student's t-test). (**C**) *Top row*: Classical active multiple sclerosis brain lesion (Case 9); *middle row*: primary inflammatory childhood CALD brain lesion (Case 2); *bottom row*: primary inflammatory adult CALD spinal cord lesion (Case 4). The columns show immunohistochemical single staining for MRP14, CD68, CD86, CD206 and CD163, as used for the quantification in **A**. Arrows point to positive cells for which magnified views are shown in the insets. (**D**) Double immunohistochemistry for CD86 and CD206 in the same regions as shown in **C**. Arrowhead points to a double-positive macrophage, representing an intermediate inflammatory phenotype, which was observed in multiple sclerosis but hardly present in the CALD cases. Arrows point to the few CD206-single-positive cells detected in multiple sclerosis and CALD. Scale bars = 50 μm; *inset* scale bars = 25 μm.
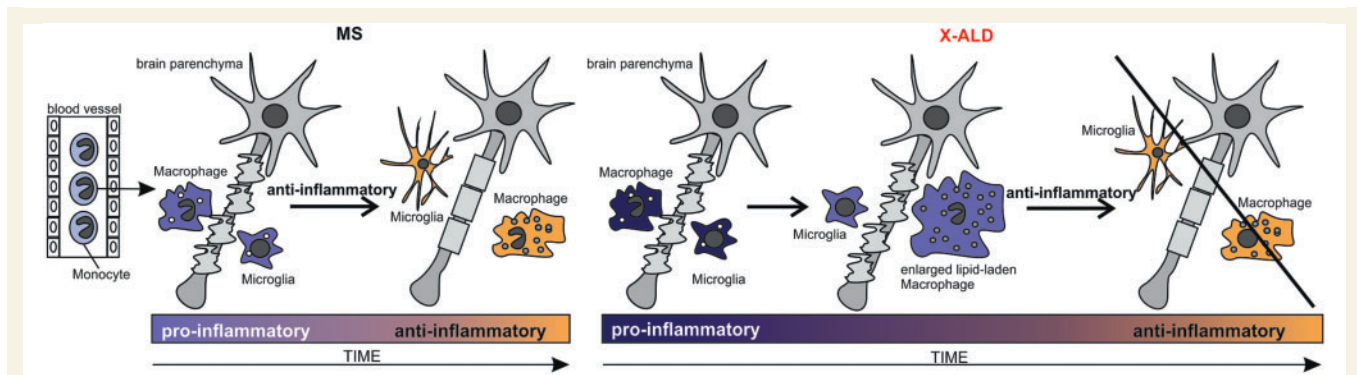
Figure 6 Hypothetical model of the progression of CALD when compared to multiple sclerosis. In CALD, a reinforced destruction of myelin occurs that could be caused by a reduced capacity of pro-inflammatory enlarged lipid-laden macrophages to clear the injured site and induce remyelination.

stated that in contrast to the relentless disease progression in CALD, multiple sclerosis typically displays a relapsing-remitting course and, thus, a considerable variability with respect to anti-inflammatory activity between multiple sclerosis lesions is expected. Accordingly, we took utmost care in selecting acute multiple sclerosis lesions that comprised comparable densities of macrophages and microglia (CD68 + cells) in general as well as similar amounts of neutral lipid-containing macrophages, in order to minimize the disease-specific pathophysiological differences between multiple sclerosis and X-ALD. Intriguingly, detailed histological analysis of the lipid-laden macrophages in CALD lesions revealed an exceptionally enlarged size and, in stark contrast to multiple sclerosis lipophages, predominantly pro-inflammatory phenotype. The ballooned appearance of the lipid-laden macrophages in CALD lesions probably reflects a reduced capacity of these cells to clear injured sites of tissue debris potentially inhibiting remyelination. Together, these findings strongly support our hypothesis that in the inflammatory form of X-ALD, a failure of macrophages to transit from the pro-inflammatory phase to the regenerative phase of repair perpetuates the destruction of myelin (Fig. 6). In addition, the success of haematopoietic stem cell transplantation or gene therapy for CALD would also be in line with this assumption, as the ABCD1-positive monocytes/macrophages derived from the donor CD34 + stem cells are able to degrade the VLCFAs enriched in the phagocytosed myelin. Thus, in the treated patients, the metabolic defect hindering transition to the anti-inflammatory remyelinating phase is presumably corrected. Although the interpretation of our results would fit the proposed hypothesis, it must be taken into account that with X-ALD being a rare disorder, only a limited set of patients could be analysed and that these, at least in the context of monocyte transcriptome analysis, displayed substantial interindividual variability.

Haematopoietic stem cell transplantation and gene therapy cannot rescue CALD patients with advanced disease progression. In addition, haematopoietic stem cell transplantation requires a well-matched donor to reduce the risk of graft-versus-host reactions and periprocedural mortality. Accordingly, these procedures can only be applied to a selected subset of patients at early stages of cerebral inflammation, whereas all other childhood and adult CALD patients are still left without treatment. So, how could a detrimental role of pro-inflammatory skewed monocytes and macrophages in X-ALD pathology be prevented? One strategy would be to correct the inherited functional defect in X-ALD macrophages by pharmacologically upregulating the homologous peroxisomal ABC transporter ABCD2 (Weinhofer *et al.*, 2002, 2005, 2008). Upon overexpression, ABCD2 is able to compensate for the lack of ABCD1 in cultured cells as well as in the X-ALD mouse model (Netik *et al.*, 1999; Pujol *et al.*, 2004). Current investigations will reveal whether induction of *ABCD2* expression in X-ALD monocytes and macrophages can revert the pro-inflammatory skewing in these cells. However, the results of the present study might also trigger research along a new alternative therapeutic avenue for X-ALD based on metabolic reprogramming of pro-inflammatory M1 macrophages. Recently it was discovered that specific metabolic processes such as glycolysis, Krebs cycle and fatty acid metabolism are strongly associated with macrophage polarization (Mills and O'Neill, 2016). Thus, pharmacological manipulation of these pathways in X-ALD macrophages could be promising for dampening the pro-inflammatory response in CALD lesions.

In summary, our results show that ABCD1 deficiency results in innate pro-inflammatory skewing of X-ALD monocytes and macrophages. In CALD, the rapid progression of myelin destruction associated with the necessity of macrophages to phagocytose the VLCFA-enriched myelin debris, despite impaired capacity to degrade these lipids, seems to cause an enormous metabolic burden on these already pro-inflammatory skewed cells. Accordingly, X-ALD macrophages divert by forming exceptionally enlarged foam cells that are incapable of switching to an anti-inflammatory activation state that would possibly be a prerequisite for stopping the destruction of myelin and initiate remyelination.

Acknowledgements

Funding

Supplementary material

Supplementary material is available at *Brain* online.

References

Anders S, Pyl PT, Huber W. HTSeq–a Python framework to work with high-throughput sequencing data. Bioinformatics 2015; 31: 166–9.

Berger J, Forss-Petter S, Eichler FS. Pathophysiology of X-linked adrenoleukodystrophy. Biochimie 2014; 98: 135–42.

Boven LA, Van Meurs M, Van Zwam M, Wierenga-Wolf A, Hintzen RQ, Boot RG, et al. Myelin-laden macrophages are anti-inflammatory, consistent with foam cells in multiple sclerosis. Brain 2006; 129 (Pt 2): 517–26.

Brück W, Porada P, Poser S, Rieckmann P, Hanefeld F, Kretzschmar HA, et al. Monocyte/macrophage differentiation in early multiple sclerosis lesions. Ann Neurol 1995; 38: 788–96.

Budka H, Sluga E, Heiss WD. Spastic paraplegia associated with Addison's disease: adult variant of adreno-leukodystrophy. J Neurol 1976; 213: 237–50.

Cartier N, Aubourg P. Hematopoietic stem cell transplantation and hematopoietic stem cell gene therapy in X-linked adrenoleukodystrophy. Brain Pathol 2010; 20: 857–62.

Ecker J, Liebisch G, Englmaier M, Grandl M, Robenek H, Schmitz G. Induction of fatty acid synthesis is a key requirement for phagocytic differentiation of human monocytes. Proc Natl Acad Sci USA 2010; 107: 7817–22.

Eichler FS, Ren JQ, Cossoy M, Rietsch AM, Nagpal S, Moser AB, et al. Is microglial apoptosis an early pathogenic change in cerebral X-linked adrenoleukodystrophy? Ann Neurol 2008; 63: 729–42.

Frischer JM, Bramow S, Dal-Bianco A, Lucchinetti CF, Rauschka H, Schmidbauer M, et al. The relation between inflammation and neurodegeneration in multiple sclerosis brains. Brain 2009; 132 (Pt 5): 1175–89.

Hametner S, Wimmer I, Haider L, Pfeifenbring S, Bruck W, Lassmann H. Iron and neurodegeneration in the multiple sclerosis brain. Ann Neurol 2013; 74: 848–61.

Harboe M. A method for determination of hemoglobin in plasma by near-ultraviolet spectrophotometry. Scand J Clin Lab Invest 1959; 11: 66–70.

Hofereiter J, Smith MD, Seth J, Tudor KI, Fox Z, Emmanuel A, et al. Bladder and Bowel dysfunction is common in both men and women with mutation of the ABCD1 gene for X-linked adrenoleukodystrophy. JIMD Rep 2015; 22: 77–83.

Kim D, Pertea G, Trapnell C, Pimentel H, Kelley R, Salzberg SL. TopHat2: accurate alignment of transcriptomes in the presence of insertions, deletions and gene fusions. Genome Biol 2013; 14: R36.

King G, Payne S, Walker F, Murray GI. A highly sensitive detection method for immunohistochemistry using biotinylated tyramine. J Pathol 1997; 183: 237–41.

Larocca JN, Norton WT. Isolation of myelin. Curr Protoc Cell Biol 2007; Chapter 3:Unit3.25. doi: 10.1002/0471143030.cb0325s33.

Mills EL, O'Neill LA. Reprogramming mitochondrial metabolism in macrophages as an anti-inflammatory signal. Eur J Immunol 2016; 46: 13–21.

Moser HW, Smith KD, Watkins PA, Powers J, Moser AB. X-linked adrenoleukodystrophy. In: Scriver CR, Beaudet AL, Sly WS, Valle D, editors. The metabolic and molecular bases of inherited disease, 8th edn. New York, NY: McGraw-Hill; 2001. p. 3257–301.

Musolino PL, Gong Y, Snyder JM, Jimenez S, Lok J, Lo EH, et al. Brain endothelial dysfunction in cerebral adrenoleukodystrophy. Brain 2015; 138 (Pt 11): 3206–20.

Netik A, Forss-Petter S, Holzinger A, Molzer B, Unterrainer G, Berger J. Adrenoleukodystrophy-related protein can compensate functionally for adrenoleukodystrophy protein deficiency (X-ALD): implications for therapy. Hum Mol Genet 1999; 8: 907–13.

Norton WT, Poduslo SE. Myelination in rat brain: method of myelin isolation. J Neurochem 1973; 21: 749–57.

Powers JM, DeCiero DP, Ito M, Moser AB, Moser HW. Adrenomyeloneuropathy: a neuropathologic review featuring its noninflammatory myelopathy. J Neuropathol Exp Neurol 2000; 59: 89–102.

Powers JM, Liu Y, Moser AB, Moser HW. The inflammatory myelinopathy of adreno-leukodystrophy: cells, effector molecules, and pathogenetic implications. J Neuropathol Exp Neurol 1992; 51: 630–43.

Prinz M, Priller J. Microglia and brain macrophages in the molecular age: from origin to neuropsychiatric disease. Nat Rev Neurosci 2014; 15: 300–12.

Pujol A, Ferrer I, Camps C, Metzger E, Hindelang C, Callizot N, et al. Functional overlap between ABCD1 (ALD) and ABCD2 (ALDR) transporters: a therapeutic target for X-adrenoleukodystrophy. Hum Mol Genet 2004; 13: 2997–3006.

Ruiz M, Jove M, Schluter A, Casasnovas C, Villarroya F, Guilera C, et al. Altered glycolipid and glycerophospholipid signaling drive inflammatory cascades in adrenomyeloneuropathy. Hum Mol Genet 2015; 24: 6861–76.

Subramanian A, Tamayo P, Mootha VK, Mukherjee S, Ebert BL, Gillette MA, et al. Gene set enrichment analysis: a knowledge-based approach for interpreting genome-wide expression profiles. Proc Natl Acad Sci USA 2005; 102: 15545–50.

Tippmann S. Programming tools: adventures with R. Nature 2015; 517: 109–10.

Turk BR, Theisen BE, Nemeth CL, Marx JS, Shi X, Rosen M, et al. Antioxidant capacity and superoxide dismutase activity in adreno-leukodystrophy. JAMA Neurol 2017; 74: 519–24.

van Roermund CW, Visser WF, Ijlst L, van Cruchten A, Boek M, Kulik W, et al. The human peroxisomal ABC half transporter ALDP functions as a homodimer and accepts acyl-CoA esters. FASEB J 2008; 22: 4201–8.

van Roermund CW, Visser WF, Ijlst L, Waterham HR, Wanders RJ. Differential substrate specificities of human ABCD1 and ABCD2 in peroxisomal fatty acid beta-oxidation. Biochim Biophys Acta 2011; 1811: 148–52.

Vogel DY, Vereyken EJ, Glim JE, Heijnen PD, Moeton M, van der Valk P, et al. Macrophages in inflammatory multiple sclerosis lesions have an intermediate activation status. J Neuroinflammation 2013; 10: 35.

Weber FD, Wiesinger C, Forss-Petter S, Regelsberger G, Einwich A, Weber WH, et al. X-linked adrenoleukodystrophy: very long-chain

fatty acid metabolism is severely impaired in monocytes but not in lymphocytes. Hum Mol Genet 2014; 23: 2542–50.

Weinhofer I, Forss-Petter S, Zigman M, Berger J. Cholesterol regulates ABCD2 expression: implications for the therapy of X-linked adrenoleukodystrophy. Hum Mol Genet 2002; 11: 2701–8.

Weinhofer I, Kunze M, Rampler H, Bookout AL, Forss-Petter S, Berger J. LXRalpha interferes with SREBP1c-mediated Abcd2 expression: novel cross-talk in gene regulation. J Biol Chem 2005; 280: 41243–51.

Weinhofer I, Kunze M, Rampler H, Forss-Petter S, Samarut J, Plateroti M, et al. Distinct modulatory roles for thyroid hormone receptors

TRalpha and TRbeta in SREBP1-activated ABCD2 expression. Eur J Cell Biol 2008; 87: 933–45.

Wiesinger C, Eichler FS, Berger J. The genetic landscape of X-linked adrenoleukodystrophy: inheritance, mutations, modifier genes, and diagnosis. Appl Clin Genet 2015; 8: 109–21.

Wiesinger C, Kunze M, Regelsberger G, Forss-Petter S, Berger J. Impaired very long-chain acyl-CoA beta-oxidation in human X-linked adrenoleukodystrophy fibroblasts is a direct consequence of ABCD1 transporter dysfunction. J Biol Chem 2013; 288: 19269–79.